

AD-A071 693

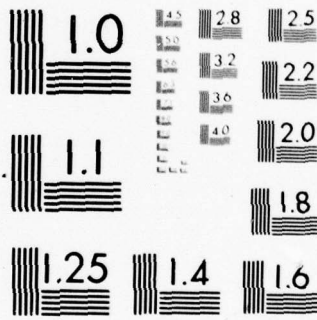
UNITED KINGDOM ATOMIC ENERGY AUTHORITY RISLEY (ENGLAN--ETC F/G 11/6  
AN INTEGRATED ELECTRON AND OPTICAL METALLOGRAPHIC METHOD FOR TH--ETC(U)  
FEB 79 G F SLATTERY, P O'RIORDAN, M E LAMBERT  
ND-R-284(R)

UNCLASSIFIED

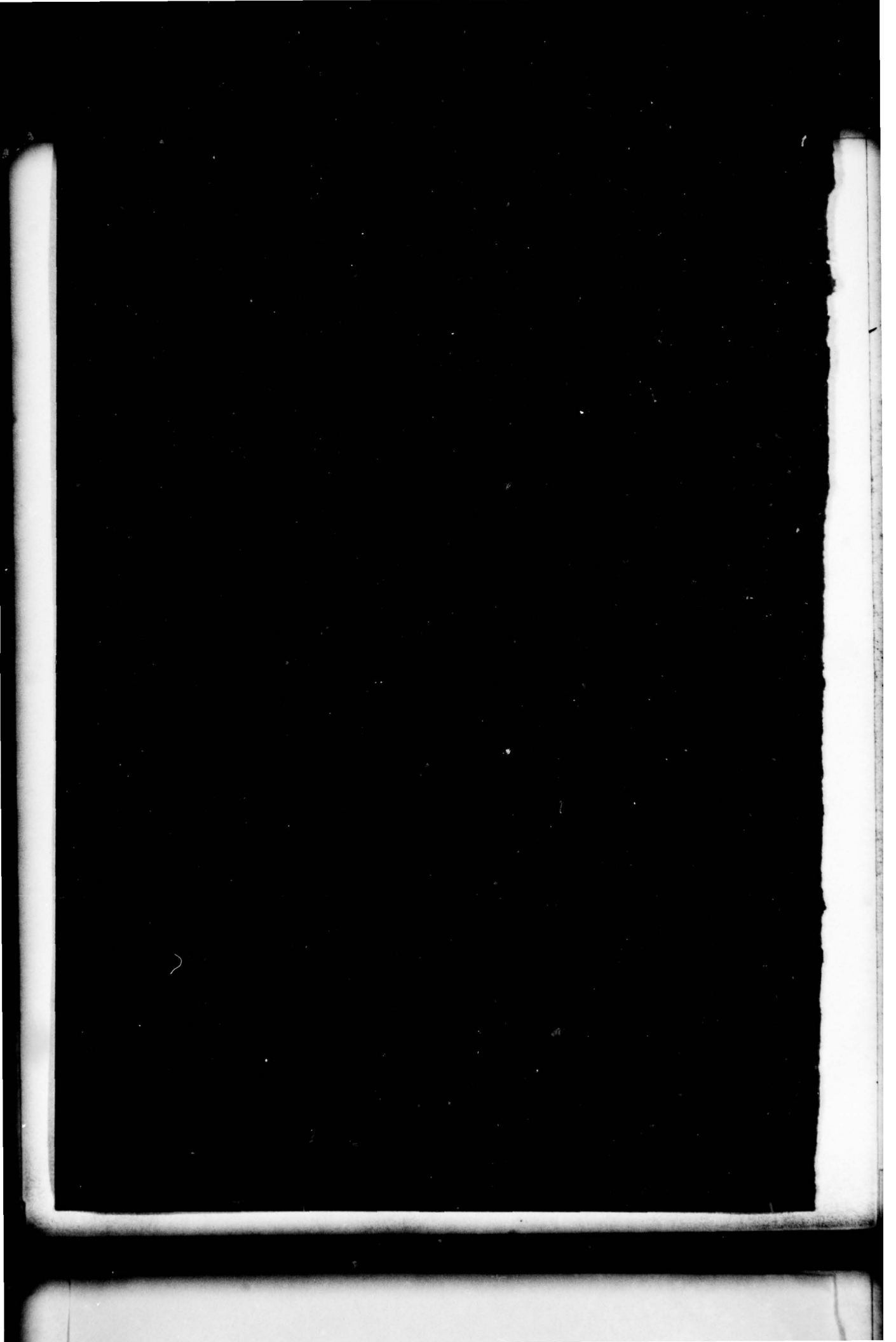
NL

| OF |  
AD  
A071693





MICROCOPY RESOLUTION TEST CHART  
NATIONAL BUREAU OF STANDARDS 1963-A



UNITED KINGDOM ATOMIC ENERGY AUTHORITY  
NORTHERN DIVISION REPORT

6  
**An integrated electron and optical metallographic method  
for the identification of phases in Type 316  
austenitic stainless steel**

by  
10 G. F./Slattery, P./O'Riordan, M. E./Lambert ~~and~~ S. M./Green  
Risley Nuclear Power Development Laboratories

SUMMARY

↓  
A sequential and integrated metallographic examination has been developed and successfully employed to differentiate between the carbide, sigma, chi, Laves and ferrite phases which are commonly encountered in Type 316 austenitic steel. The experimental procedures of optical and electron microscopy to identify these phases have been outlined and provide a rapid and convenient method of characterising the microstructure of the steel. The examination has highlighted significant cast-to-cast variations in the microstructures of consequence to the performance of the steel in service. ↗

Accession For	
NTIS GRA&I	<input checked="" type="checkbox"/>
DDC TAB	<input type="checkbox"/>
Unannounced	<input type="checkbox"/>
Justification	
By _____	
Distribution/	
Availability Codes	
Dist	Avail and/or special
A	

11 February 1979

12 30p.

DDC  
RECEIVED  
JUL 26 1979  
REGULATED  
D

411 297

LB

29 07 23 218

## CONTENTS

	Page
1. INTRODUCTION	3
2. EXPERIMENTAL PROCEDURE	3
3. MATERIALS EXAMINED	4
4. RESULTS	5
4.1 Control samples	5
4.2 Service samples	6
5. DISCUSSION	6
6. CONCLUSIONS	7
7. REFERENCES	8
TABLE 1	9
FIGURES 1-21	

## 1. INTRODUCTION

The microstructural changes which take place in Type 316 stainless steel at elevated temperatures are of considerable technological interest since they can influence the mechanical and chemical properties of the steel. The major precipitate phases reported for this steel<sup>(1-9)</sup> are  $M_{23}C_6$  carbide, chi ( $\chi$ ), sigma ( $\sigma$ ), Laves ( $\eta$ ) and ferrite with  $M_6C$  present in minor amounts. In view of the complex nature of phase formation in this alloy<sup>(1)</sup> there is a need for experimental techniques which are capable of rapid and unambiguous phase identification so that detailed studies of microconstituents can be made in relation to the temperature and time characteristics experienced in service.

It is advisable to commence such studies using optical microscopy since this is the most satisfactory method for revealing the precipitate morphology and distribution in the bulk sample. However positive identification by the optical microscope tends to be somewhat subjective and unreliable owing to the uncertainties associated with etching techniques. In addition, the resolution available with the optical microscope imposes a restriction on the ability to observe clearly the smaller precipitate particles. Consequently, it is customary to supplement optical microscopy with electron microscopy and X-ray analysis which however tend to be rather time consuming and therefore less convenient for a comprehensive microcharacterisation of the bulk material.

An integrated sequential metallographic examination has been evolved to optimise the benefits to be gained from all these techniques. The sequence commences with Nomarski interference contrast examination of the as-polished specimen, continues with scanning electron microscopy coupled with energy dispersive X-ray spectrometry, followed by selective etching of the specimen and further optical microscopy and finally transmission electron microscopy in both the conventional and scanning modes for diffraction and micro-analysis of the precipitates. This Report describes the application of this integrated approach to the microcharacterisation of some of the more commonly encountered phases in Type 316 steel after thermal ageing for various times in the temperature range 600° to 850°C.

## 2. EXPERIMENTAL PROCEDURE

The samples are sectioned and prepared for examination by conventional grinding and polishing with one micron diamond paste. Final relief polishing is performed using gamma alumina. It is necessary to achieve the best possible relief polish in order to avoid scratch marks which otherwise would appear exaggerated using the Nomarski interference contrast technique. This technique is based on the interference of two sets of light waves produced in a birefringent quartz plate above the objective. The incident plane polarised light is split into two mutually perpendicular plane polarised components such that a double image of the specimen surface is obtained with a small lateral shift between the two images. The path length of the two beams is identical, and by using an analyser, they can be made to interfere whenever features in the two images fail to coincide. The Nomarski technique is ideal for the examination of very slight changes in level of features in the specimen surface. Consequently, it is ideal for revealing the presence of precipitate particles in the as-polished condition prior to etching. Microhardness indentations and scratches can be used to locate areas of interest before transferring the specimen to the scanning electron microscope (SEM) for further observation and analysis of the identical specimen region.

The samples are then examined in the S4-10 Cambridge SEM coupled with a Tracor 880 analysis system and using an incident electron beam voltage of 20 kV. An in-situ examination is made on particles previously selected for study by Nomarski interference contrast imaging and the phases identified by the Weiss et al intensity ratio technique<sup>(10)</sup> in which the particles are grouped according to their characteristic Mo/Cr and Fe/Cr X-ray intensity ratios. Since the spatial resolution for analysis is degraded significantly compared with the incident beam diameter due to electron scatter beneath the specimen surface, this method is more suitable for the relatively larger particles, ideally one micron and above, if an X-ray contribution from the matrix is to be avoided.

The analytical data from the SEM/EDS (energy dispersive spectroscopy) examination are then correlated with the results of metallographic etching and bright field optical microscopy to provide an identification based on etching response. It is feasible using colour etching techniques to differentiate between the various micro-constituents in stainless steel provided the microstructural features are fully exposed by means of a general etchant prior to the application of the colour reagent. Thus LeMay and

White<sup>(11)</sup> claim that Murakami and Groesbeck's reagents if applied very carefully, will differentiate satisfactorily between carbides, sigma and ferrite co-existing in the same austenitic matrix provided the particle size is within the resolving power of the microscope. However it appears that unless the characteristic colours are slowly and uniformly built-up, staining and poor discrimination between the various micro-constituents can result. Weiss et al<sup>(10)</sup> point out that attempts to distinguish between the intermetallic phases in Type 316 steel are often unsuccessful. They found that a light micrograph of a specimen containing mainly sigma and chi phases looked essentially like a micrograph containing predominantly  $M_{23}C_6$  carbide and only a small amount of intermetallic phases. Hence colour etching appears somewhat inconsistent in operation and is also not suitable for use with oil immersion lenses at high magnification. Consequently, it was decided to develop a selective etching technique in which particle recognition for all the phases is dependent on the rate of attack of the particle in the etchant. The method used was electrolytic etching in ten percent oxalic acid at 5 volts using a stainless steel cathode. With experience, it is possible to recognise the various microconstituents on the basis of their etching characteristics and by examination of the same particles previously identified in the SEM, to obtain a correlation between particle X-ray analysis and etching response.

As a final step in the sequence, confirmatory evidence to support the previous findings is obtained from thin foil electron microscopy. Thin foils were prepared by electrochemical polishing in a Tenupol unit using an electrolyte of 6 percent perchloric acid and 94 percent glacial acetic acid at 13°C. Both conventional and scanning transmission electron microscopy were carried out on a JEOL 100C microscope operated at 100 kV and fitted for microanalysis with an energy-dispersive X-ray spectrometer. The precipitate particles were located and imaged in the STEM mode where the electron beam is focused to a small spot size and either scanned over the field of view or maintained stationary as a fine probe for microanalysis, Fig. 1. An improved X-ray spatial resolution is possible with thin foils where beam spreading effects are small. The foil is tilted from the horizontal towards the X-ray detector to facilitate the collection of X-rays. The individual particles observed in the foils are characterised by the intensity ratio technique of Weiss et al<sup>(10)</sup> in the same manner as the SEM examination of particles in the bulk sample. Chemical identification in a more quantitative sense is obtained by the Cliff and Lorimer method<sup>(12,13)</sup> which assumes that for very thin foils, the effects due to X-ray absorption and fluorescence can be neglected. In this method, the ratio of two characteristic X-ray intensities of elements A and B is related to the corresponding weight fraction ratios,  $C_A/C_B$ , by the expression  $C_A/C_B = K_{AB} I_A/I_B$ , where  $K_{AB}$  is a constant at a given accelerating voltage. Provided  $I_A$  and  $I_B$  are measured simultaneously,  $K_{AB}$  is independent of the beam current and variation in specimen thickness. Thus a pair of weight fraction ratios can be obtained from the X-ray intensity ratios provided the value of  $K$  is known. Details of the computational procedures have been reported previously.<sup>(14)</sup> Diffraction patterns are obtained and indexed using the equation  $\lambda L = rd$  where  $\lambda$  is the wavelength of the electrons,  $L$  the camera length,  $r$  the spacing of the reciprocal lattice spots in the diffraction pattern and  $d$  is the interplanar spacing corresponding to the series of atomic planes giving rise to the reciprocal lattice spot at spacing  $r$ . Knowing the value of the camera constant  $\lambda L$ , the  $d$  value of the particles can be calculated and compared to tabulated lists of  $d$  spacings for the various phases found in the steel. When the X-ray intensity method is used in conjunction with electron diffraction analysis, the identification of the precipitate phases can be ascertained unambiguously.

### 3. MATERIALS EXAMINED

Samples of Type 316 steel were selected to provide examples of the more commonly encountered phases present in significant amounts in the steel. These 'control' samples were chosen both from practical experience of this alloy system and also from reference to published literature as being likely to provide suitable amounts of the major phases for study and this supposition was checked by detailed electron microscopy and X-ray analysis of the 'controls'. The conditions were chosen as follows:-

(i) For FERRITE in Type 316 weld metal

Type 316 steel under equilibrium conditions should be wholly austenitic in character but weld metal is so alloyed that it contains a few percent of ferrite remaining in the structure to prevent hot cracking of the weld. The presence of ferrite is associated with the rapid cooling of the weld metal and the sluggish nature of the peritectic reaction involved.<sup>(15)</sup> The ferrite is enriched in chromium and molybdenum and impoverished slightly in nickel.

It is distributed in a characteristically vermicular form throughout the austenite matrix<sup>(16)</sup> and possesses a body-centred cubic structure with lattice parameter  $a_0 = 2.866 \text{ \AA}$  in contrast to the austenite matrix which is face-centred cubic with  $a_0 = 3.598 \text{ \AA}$ . The chemical composition of the weld metal is given in Table 1.

- (ii) For  $M_{23}C_6$  CARBIDE and CHI-PHASE in solution-treated Type 316 steel thermally aged at  $800^\circ\text{C}$  for 1000 hours and containing carbide precipitates together with chi-phase.<sup>(11,14)</sup> Details of the crystal structure of  $M_{23}C_6$  and chi have been reported previously.<sup>(14)</sup> The chemical composition of the steel is given in Table 1 (item 59).
- (iii) For SIGMA in 20% cold worked M316 steel creep tested at  $700^\circ\text{C}$  and  $41.5 \text{ N/mm}^2$  to a total strain of 1.06% in 10,832 hours. The composition of this steel is given in Table 1. Information on sigma phase has been well documented in the literature, for example the review by Hall and Algie.<sup>(17)</sup> It is an intermetallic phase of electron-compound type with a tetragonal crystal structure having 30 atoms per unit cell and a c/a parameter ratio of 0.52. The lattice parameters of sigma-phase chemically extracted from Type 316 steel after ageing at  $815^\circ\text{C}$  for 3000 hours were determined as  $a_0 = 8.828 \pm 0.002 \text{ \AA}$  and  $c_0 = 4.597 \pm 0.002 \text{ \AA}$ .<sup>(11)</sup>

Having developed the process of sequential examination on the above 'control' standards, the method was applied to a diverse series of specimens of practical interest in order to check the phases present. These specimens were chosen as follows:

- (a) Solution treated Type 316 steel aged at  $650^\circ\text{C}$  for 22,800 hours. This long term treatment sample was taken from the undeformed head of a creep rupture specimen.
- (b) Type 316 weld metal stress relieved at  $850^\circ\text{C}$  for 6 hours.
- (c) As-received solution-treated Type 316 steel containing stringers of prior delta-ferrite in the austenite matrix (although under equilibrium conditions, this steel is wholly austenitic, it is not uncommon to observe ferrite stringers due to local segregation effects). The composition is given in Table 1 (Pedigree 2).
- (d) As for Item (c) but taken from a different cast of steel in which the ferrite stringers appeared to have transformed to sigma phase. The composition of this cast (Pedigree 1) is also given in Table 1.
- (e) Type 316 steel thermally aged at  $800^\circ\text{C}$  and containing examples of all four precipitate phases  $M_{23}C_6$ , sigma, chi and molybdenum containing Laves.

## 4. RESULTS

### 4.1 Control samples

Nomarski interference contrast images of typical precipitate particles found in the as-polished control samples are shown in Fig. 2. These show

- (i) a delta-ferrite distribution in the austenite matrix of the Type 316 weld metal.
- (ii) grain boundary sigma phase in cold worked M316 steel.
- (iii) grain boundary chi phase and carbide in thermally aged Type 316 steel.

The identical areas observed in the SEM are shown in Fig. 3 (these are mirror images to the optical micrographs) together with the characteristic X-ray emission spectra and the corresponding intensity ratios for the Mo/Cr and Fe/Cr peaks. On this basis, it is possible to differentiate between the four precipitate phases and to correlate this identification with the interference contrast optical images.

The results of electrolytic etching the same areas are given in Fig. 4. Carbides are affected first by the oxalic acid etch which attacks the chromium depleted/modified austenite zone surrounding the carbide particle thereby causing the smaller particles to drop out. Next, the etchant attacks the sigma particles themselves and the sigma can be completely dissolved after 1 second in the 10% solution. These etching times can be extended by diluting the oxalic acid solution and reducing the voltage so that it is possible to retain the smaller carbide particles in-situ with a very light etch. Chi-phase is out-

lined between 1 and 5 seconds in 10% solution but will withstand etching attack for up to 30 seconds before eventually dissolving. Ferrite phase is comparatively resistant to the etchant; the ferrite/austenite interface is outlined between 5 and 10 seconds but the particle shows no sign of dissolving after 30 seconds.

The identification of the various precipitates found in the control samples was further confirmed by the combined use of electron diffraction and energy-dispersive X-ray microanalysis using transmission electron microscopy. Typical electron micrographs, diffraction patterns and X-ray emission spectra for carbide, sigma (Fe-Cr), chi-phase and ferrite are given in Figs 5 to 8.

## 4.2 Service samples

The integrated metallographic method was applied to the service samples as follows:

(a) Solution treated 316 Type steel aged at 650°C for 22,800 hours

Large grain boundary particles were observed in this specimen. Etching in oxalic acid revealed that these grain boundary precipitates were sigma phase, Fig. 9, and this result was confirmed in the SEM examination by the Mo/Cr and Fe/Cr intensity ratios.

(b) Stress relieved weld metal

Although the second phase in the weld metal was originally delta-ferrite, the stress relieving treatment at 850°C for 6 hours could induce transformation of this ferrite. The etched microstructure Fig. 10, showed that in this region of the weld, the ferrite had substantially transformed to sigma phase as a result of the thermal treatment, and this interpretation was confirmed by the X-ray micro-analysis results.

(c) Solution treated steel containing stringers of prior delta-ferrite

Although the stringers were originally delta-ferrite, the etched structure revealed a difference between stringers in the same specimen, Fig. 11. Some stringers remained resistant to the etchant indicating a stable ferrite structure whilst others etched as sigma phase formed as a result of transformation of the ferrite. The difference in structure between the two types of stringer in the same specimen was confirmed by micro-analysis.

(d) A further cast of steel in which the stringers had transformed to sigma phase, Fig. 12. There was no evidence of untransformed ferrite in this cast indicating possible differences in microstructure between the two casts.

(e) Type 316 steel thermally aged at 800°C for 1000 hours

This specimen contained a complex distribution of precipitate phases as shown in the Nomarski image of the as-polished section, Fig. 13. The SEM image of the same field is shown in Fig. 14 (the picture shown is the mirror image of the Nomarski). Individual particles have been analysed and tabulated in terms of phases and particles of carbide, sigma, chi and Laves were all found in the same field under the microscope. Figures 15 and 16 show a lightly etched and normally etched microstructure of the same field to differentiate between carbide and sigma (the light etching retains the small carbide particles in-situ). Figure 17 shows the structure after normal etching for 3 seconds when the large sigma particles are completely dissolved and the chi phase particles only outlined. A few small particles were considered to be Laves phase which required long etching times to reveal the particles, compare Figs 17 and 18. The presence of these Laves particles was confirmed by transmission electron microscopy and a diffraction pattern and X-ray micro-analysis spectrum of Laves phase are shown in Fig. 19. A scanning transmission electron micrograph (STEM) of material from this same cast of steel, Fig. 20, shows similar features to the SEM and Nomarski micrographs. A feature of the presence of Laves phase is that it is seen to grow in contact with carbide phase, Fig. 21.

## 5. DISCUSSION

In order to characterise the microstructure of any material, it is necessary to study microscopically large representative areas of the bulk material and to image and classify areas of interest

rapidly and conveniently. Etching provides the normal method of revealing the microstructure but in many respects, etching is not suitable as a preparatory step to microanalysis with the SEM since it can cause pitting of particles and their eventual dropping out of the surface completely. There is also the possibility of stain contamination on the particle surface from the etching solution which may interfere with the analysis. Consequently, it is preferable to examine the as-polished section but under normal illumination in the optical microscope, it is difficult to image the microstructure satisfactorily. The restriction can be overcome by the use of Nomarski interference contrast techniques which are ideal for revealing particle distribution without recourse to etching. In this way, the major microconstituents found in Type 316 steel, namely carbide, sigma, chi and ferrite can be differentiated and rapidly identified using the combined techniques of optical microscopy with selective etching and scanning electron microscopy plus energy dispersive analysis of polished surfaces. The SEM provides an important extension of the optical microscope for this type of work since it is capable of imaging areas of interest at higher resolution and magnification than is possible with the optical microscope and it can also provide in-situ micro-analysis of individual particles. It can provide a qualitative guide to phase identification very quickly in an established alloy system such as Type 316 steel. The SEM is however more suitable for the rapid identification of particles greater than 1 micron size such as the large grain boundary sigma particles found in this steel. Particles less than 1 micron size can be observed and identified in a qualitative sense although there tends to be a scatter in the intensity-ratios for the smaller particle sizes caused by matrix contribution effects. Fortunately the smaller carbide particles are easy to identify since carbide phase has a chromium X-ray peak greater than that of iron (i.e. Fe/Cr ratio less than unity) and consequently it is easy to differentiate from the intermetallic phases. Even so, unfortunately, the energy-dispersive method does not provide a direct assessment of carbon content.

Transmission electron microscopy either on thin foils or extraction replicas provides an important supplement to optical and scanning microscopy on bulk specimens particularly since matrix effects and ZAF corrections are avoided so that smaller particles (less than 1 micron) can be examined with confidence. The ability to provide a similar EDS spectrum to that obtained with the SEM but coupled with electron diffraction capability provides a powerful tool for studying individual particles especially within the smaller ranges. The quantitative data on Mo/Cr and Fe/Cr intensity ratios for thin foil microscopy are in reasonable agreement with similar results using the SEM with bulk specimens. However since the composition of the phases may vary within a limited range, the use of the energy-dispersive method alone may lead to some degree of overlap in results between different intermetallic phases, and hence it is important to obtain electron diffraction data on crystal structure to support the X-ray micro-analysis results.

The examination has highlighted important differences in microstructure between material taken from different casts of Type 316 steel. The cast-to-cast variation is significant particularly with respect to prior-ferrite stringer and inclusion content. Thus, the ferrite has been observed in certain circumstances to transform fairly readily to sigma phase. It is therefore advisable to characterise each cast of steel microstructurally using this integrated approach of optical and electron microscopy if the subsequent mechanical and chemical behaviour of the steel is to be properly understood.

## 6. CONCLUSIONS

1. Nomarski interference contrast optical microscopy combined with scanning electron microscopy and energy-dispersive X-ray spectrometry provide a versatile and sophisticated method for the imaging and identification of precipitate phases commonly encountered in Type 316 austenitic steel.
2. Correlation of these techniques with sequential etching behaviour in oxalic acid provides a rapid and simple optical method of characterising these precipitates in a bulk sample.
3. Confirmatory information can be obtained on thin foils and extraction replicas using scanning transmission electron microscopy (STEM) plus energy-dispersive X-ray spectrometry and in conjunction with electron diffraction. The combined use of diffraction and micro-analysis enables these phases to be identified unambiguously.
4. The scanning electron microscope (SEM) is most useful for particles greater than 1 micron in size where matrix contribution effects in the bulk sample may be small and is therefore ideal for the examination of the larger intermetallic particles of sigma and chi phase. The transmission

electron microscope with its fine electron spot size is ideally suited to the examination of the smaller particles such as grain boundary carbide since with thin foil specimens or extraction replicas, matrix effects and complicated ZAF correction procedures may be avoided.

5. There are important cast-to-cast variations in the microstructure of the Type 316 steel which could be significant to its mechanical and chemical behaviour in service.

## 7. REFERENCES

1. WEISS, B. and STICKLER, R. Phase instabilities during high temperature exposure of 316 austenitic stainless steel. *Metallurgical Transactions*, vol. 3, no. 4, 1972, p.851
2. SPRUIELL, J. E., SCOTT, J. A., ARY, C. S. and HARDIN, R. L. Microstructural stability of thermal-mechanically pretreated Type 316 austenitic stainless steel. *Metallurgical Transactions*, vol. 4, no. 6, 1973, p.1533
3. LEVEQUE, R., MERCIER, A., DEMESTRE, J., ANDRE, J. P., CALVET, J. and LEBRET, P. Etude du comportement mécanique d'aciers inoxydables austenitiques au molybdène après maintien de longue durée à chaud. *Revue de Metallurgie*, April 1971, p.275
4. WHITE, W. E. and LE MAY, I. Metallographic observations on the formation and occurrence of ferrite, sigma phase, and carbides in austenitic stainless steels. Part 2: Studies of AISI Type 316 Stainless Steels. *Metallography*, vol. 3, 1970, p.51
5. WHITE, W. E. and LE MAY, I. Metallographic observations on the formation and occurrence of ferrite, sigma phase and carbides in austenitic stainless steels, Part 3: Electron microscopy studies. *Metallography*, vol. 5, 1972, p.333
6. WHITE, W. E. and LE MAY, I. A microstructural analysis of two AISI Type 316 austenitic stainless steels. *Microstructural Science*, vol. 2, 1974, p.49
7. DUHAJ, P., IVAN, J. and MAKOVICKY, E. Sigma-phase precipitation in austenitic steels. *Journal of the Iron and Steel Institute*, vol. 206, 1968, p.1245
8. BLENKINSOP, P. A. and NUTTING, J. Precipitation of the sigma phase in an austenitic steel. *Journal of the Iron and Steel Institute*, September 1967, p.953
9. MIMINO, T., KINOSHITA, K., SHINODA, T. and MINEGISHI, I. The changes of structure and mechanical properties of 18-8 series stainless steels after prolonged ageing. *Transactions of the Iron and Steel Institute of Japan*, vol. 9, 1969, p.472
10. WEISS, B., WESLEY HUGHES, C. and STICKLER, R. SEM-techniques for the microcharacterisation of metals and alloys, part 11. *Praktische Metallographie*, vol. 8, 1971, p.528
11. LE MAY, I. and WHITE, W. E. On the use of colour etching techniques for stainless steels. *Praktische Metallographie*, vol. 4, 1969, p.53
12. CLIFF, G. and LORIMER, G. W. Quantitative analysis of thin metal foils using EMMA-4, the ratio technique. *Proceedings of the Fifth European Congress on Electron Microscopy*. Institute of Physics, London, 1972, p.140
13. CLIFF, G. and LORIMER, G. W. The quantitative analysis of thin specimens. *Journal of Microscopy*, vol. 103, 1975, p.203
14. SLATTERY, G. F., O'RIORDAN, P. and GREEN, S. M. The formation of  $M_{23}C_6$  carbide and chi-phase in thermally aged Type 316 stainless steel. ND-R-182(R)
15. ASTROM, H., LOBERG, B., BENGTSSON, B. and EASTERLING, K. E. Hot cracking and micro-segregation in 18-10 stainless steel welds. *Metal Science*, vol. 10, no. 7, 1976, p.225
16. TAKALO, T., SUUTALA, N. and MOISIO, T. Influence of ferrite content on its morphology in some austenitic weld metals. *Metallurgical Transactions*, vol. 7A, 1976, p.1591
17. HALL, E. O. and ALGIE, S. H. The sigma-phase. *Metallurgical Reviews*, vol. 11, 1966, p.61.

TABLE 1

Chemical composition of Type 316 steel and weld metal investigated

	C	Cr	Ni	Mo	Mn	Si	S	P	Ti	Fe
Weld metal	0.043	17.1	10.8	2.34	1.22	0.33	0.001	0.027	-	Balance
Item 59	0.063	17.04	10.3	2.47	0.46	0.28	0.03	0.037	-	Balance
M316	0.038	17.3	13.8	2.41	1.8	0.62	0.005	< 0.01	-	Balance
Item c Pedigree 2 }	0.04	17.2	11.3	2.70	1.64	0.65	0.008	0.027	-	Balance
Item d Pedigree 1 }	0.04	17.6	12.8	2.57	1.57	0.48	0.026	0.032	0.01	Balance

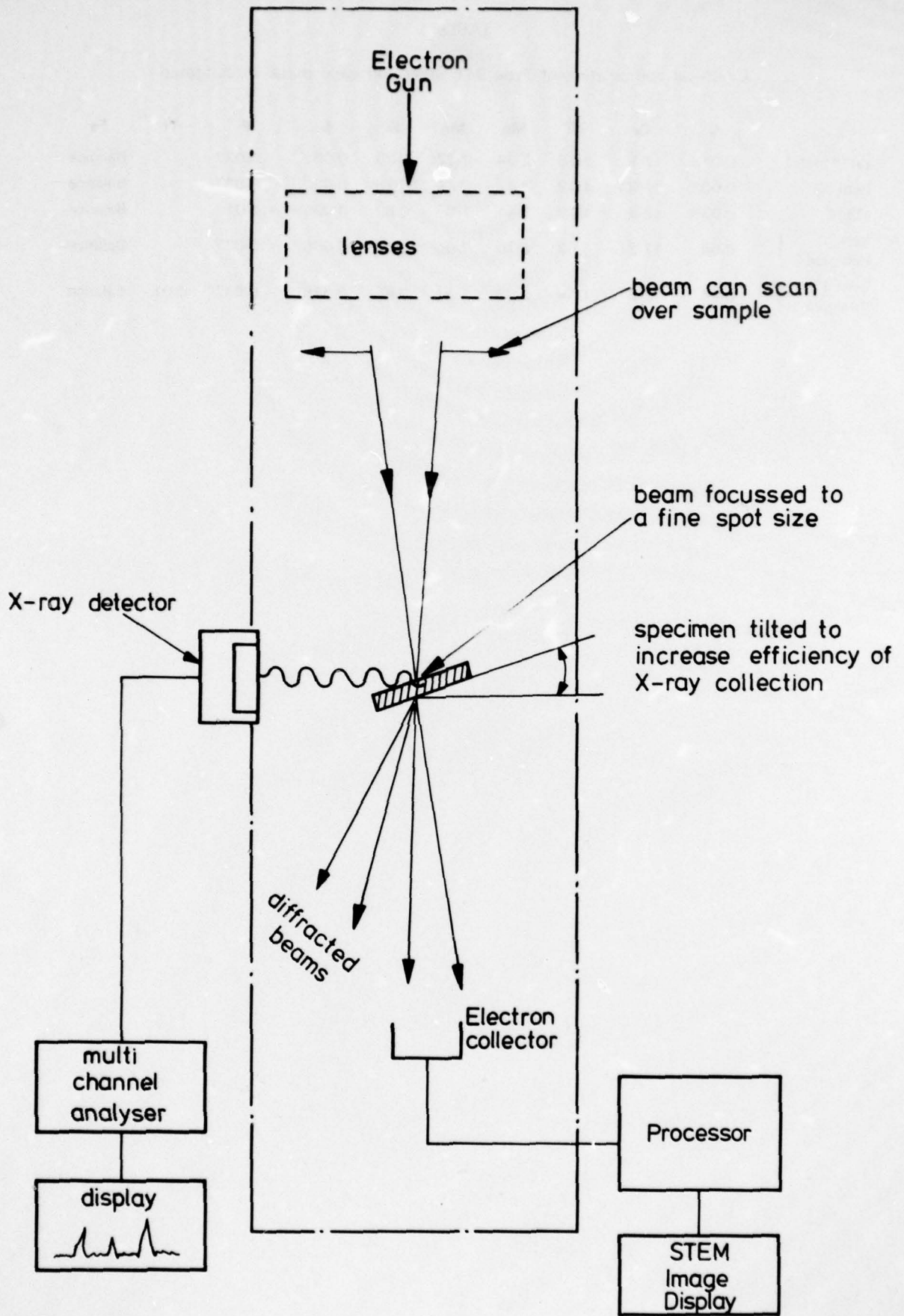
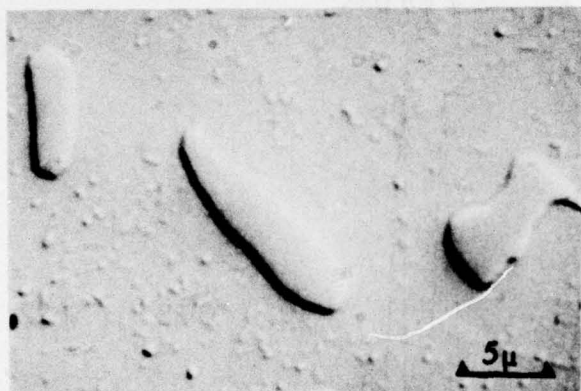


FIG.1 Schematic diagram of STEM with X-ray analyser



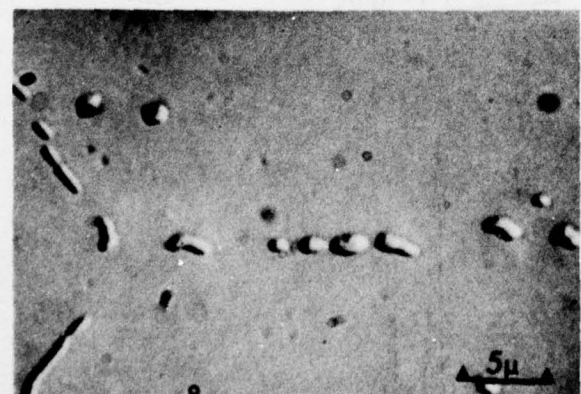
Ferrite in weld metal



Grain boundary  
Sigma phase in cold  
worked M316 ss



Grain boundary  
Chi phase in  
thermally aged  
316ss



Grain boundary  
Carbide in  
thermally aged  
316 ss

FIG 2 PRECIPITATE PHASES FOUND IN AS POLISHED SECTIONS OF 316 ss - NOMARSKI INTERFERENCE CONTRAST

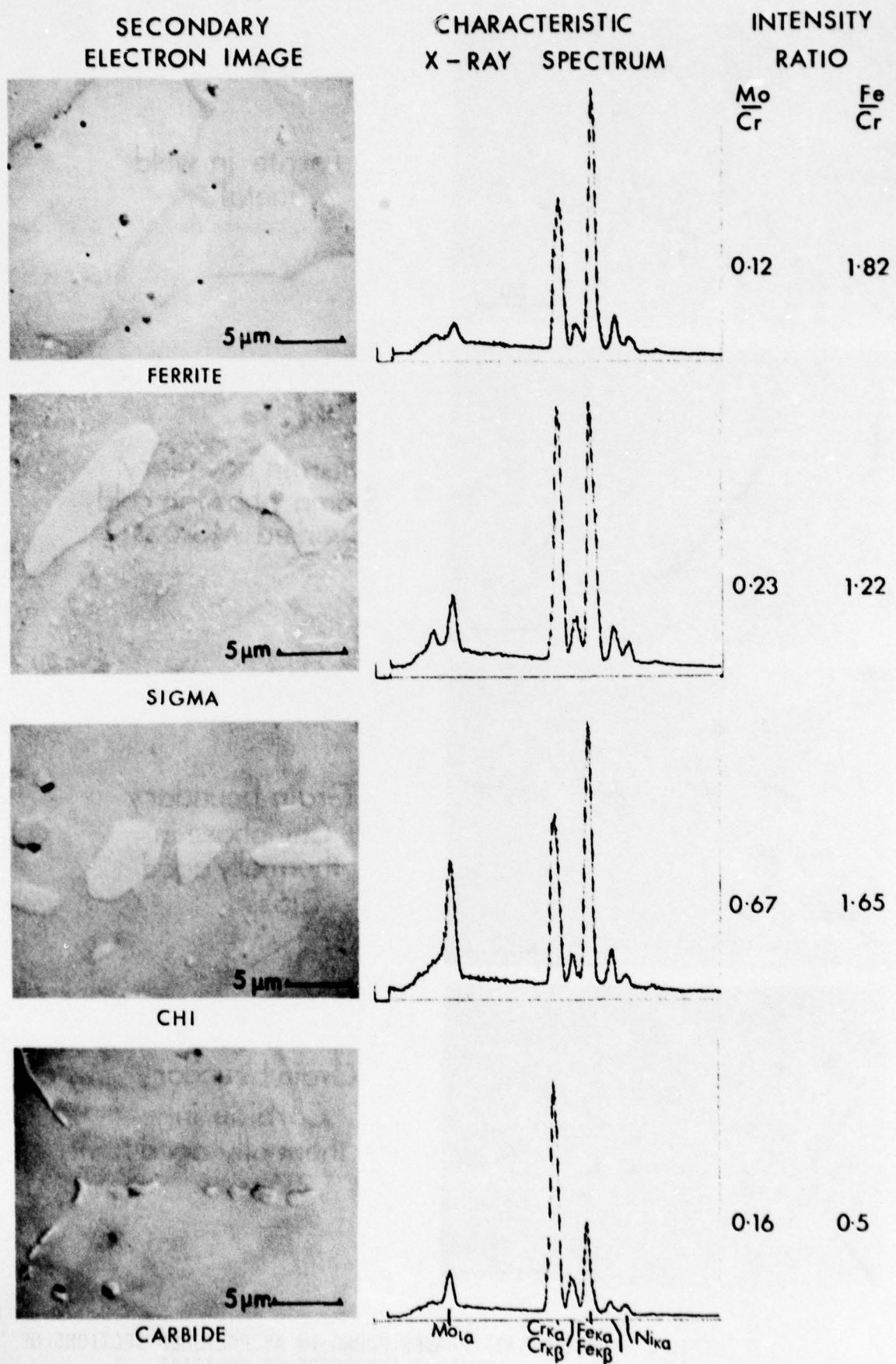
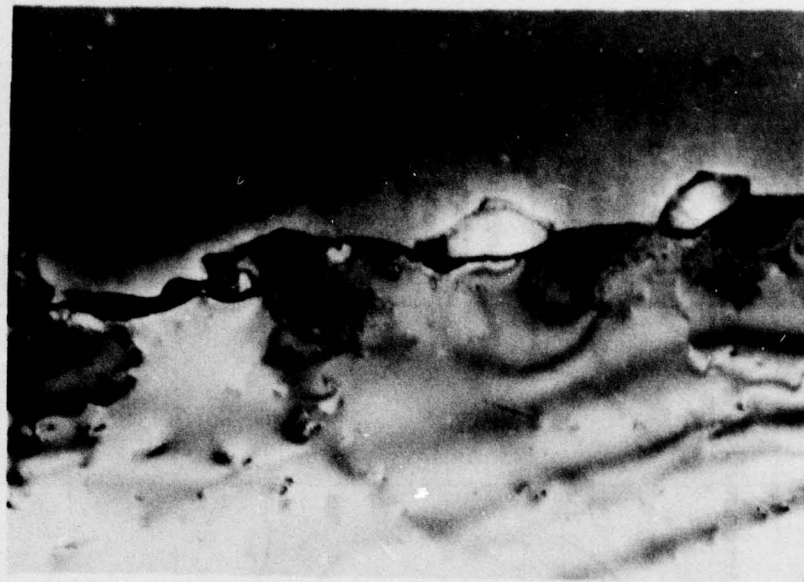


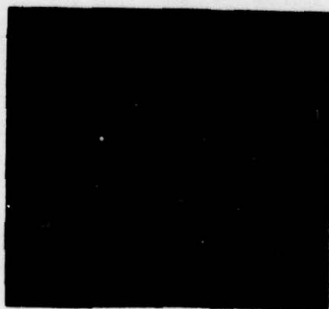
**FIG 3** PRECIPITATE PHASES FOUND IN AS POLISHED SECTIONS OF 316 ss - SECONDARY ELECTRON IMAGES AND CHARACTERISTIC X-RAY EMISSION SPECTRA

PHASE	NOMARSKI as polished 5μ	ELECTROLYTICALLY ETCHED AT 5VOLTS IN 10% OXALIC ACID						REMARKS
		0-1/2 second	1/2 1second	1-5 seconds	5-10 seconds	10-20 seconds	20-30seconds	
ferrite								ferrite outlined via attack at austenite interface
sigma								sigma dissolves completely after 1 second
chi								chi phase more resistant to etchant than sigma, outlined and eventually dissolved
carbide								etchant attacks modified austenite around carbides allowing smaller particles to drop out

FIG 4 ETCHING SEQUENCE FOR PRECIPITATES IN 316 ss USING 10% OXALIC ACID



1 $\mu$



Z A 100

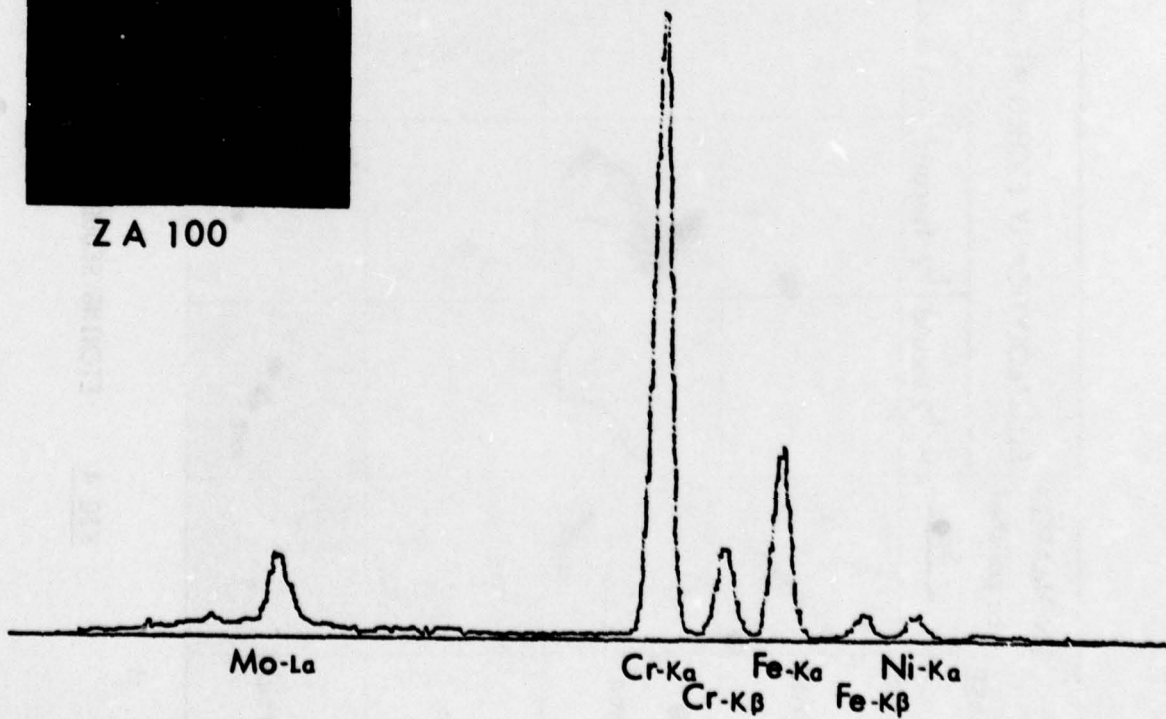
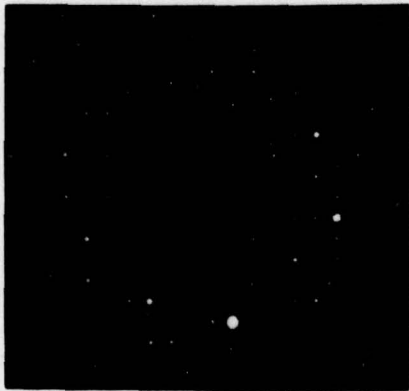


**FIG 5** TYPICAL ELECTRON MICROGRAPH, DIFFRACTION PATTERN AND X-RAY ANALYSIS SPECTRUM OF CARBIDE IN 316 ss



1 $\mu$



ZA 100

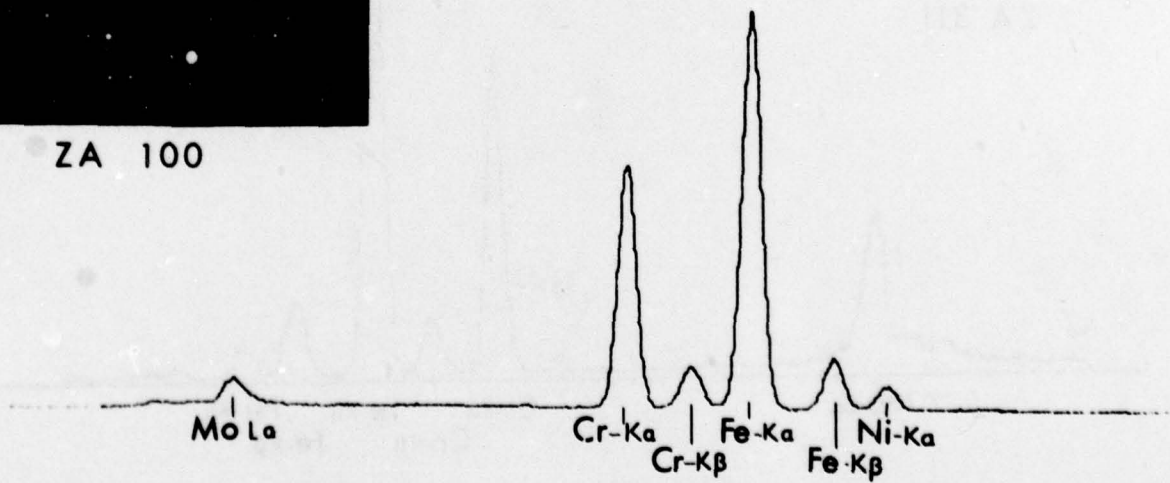
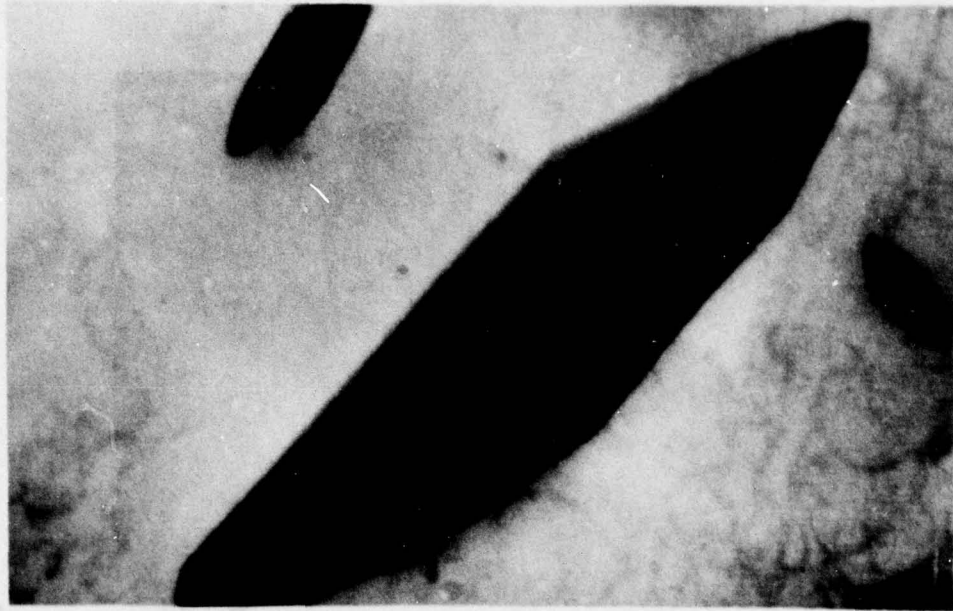
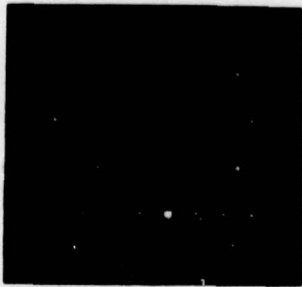


**FIG 6** TYPICAL ELECTRON MICROGRAPH, DIFFRACTION PATTERN AND X-RAY ANALYSIS SPECTRUM OF SIGMA (FeCr) PHASE IN 316 ss



1 $\mu$



ZA 311

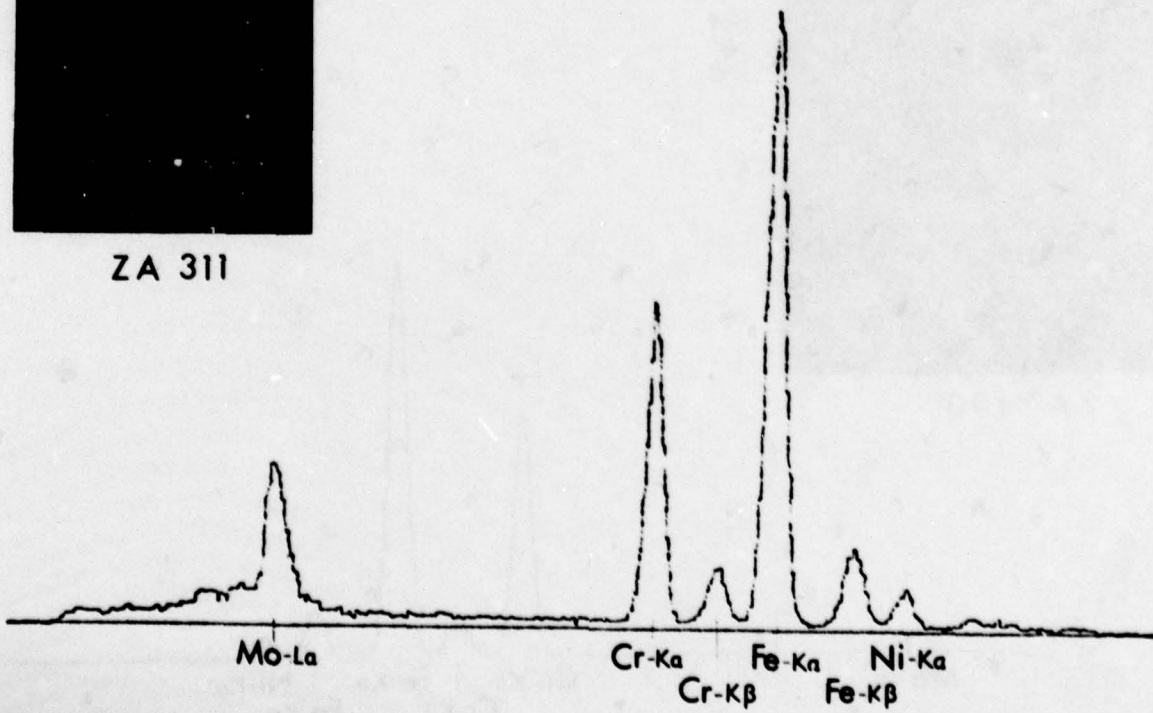
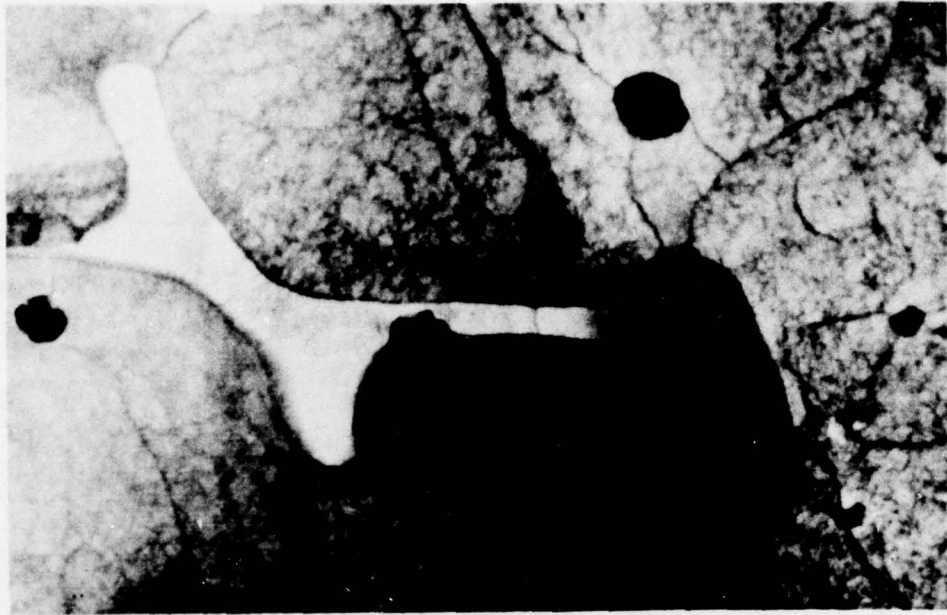
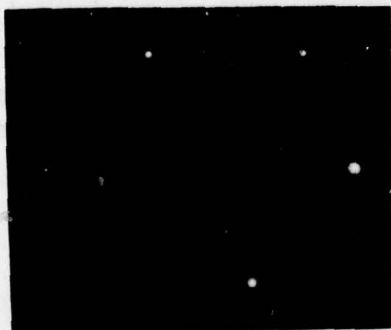


**FIG 7** TYPICAL ELECTRON MICROGRAPH, DIFFRACTION PATTERN AND X-RAY ANALYSIS SPECTRUM OF CHI-PHASE IN 316 ss



1μ



ZA 210

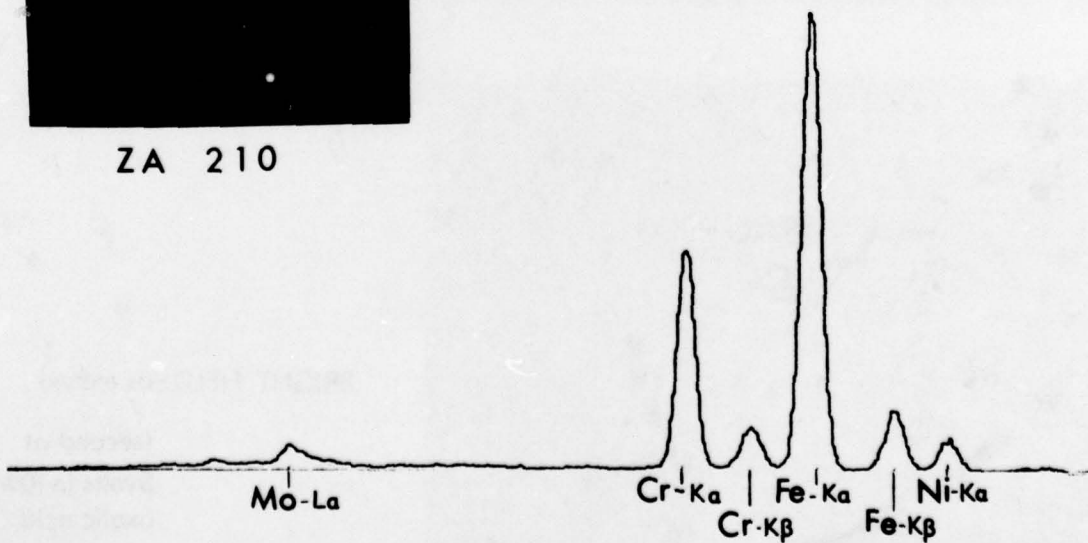
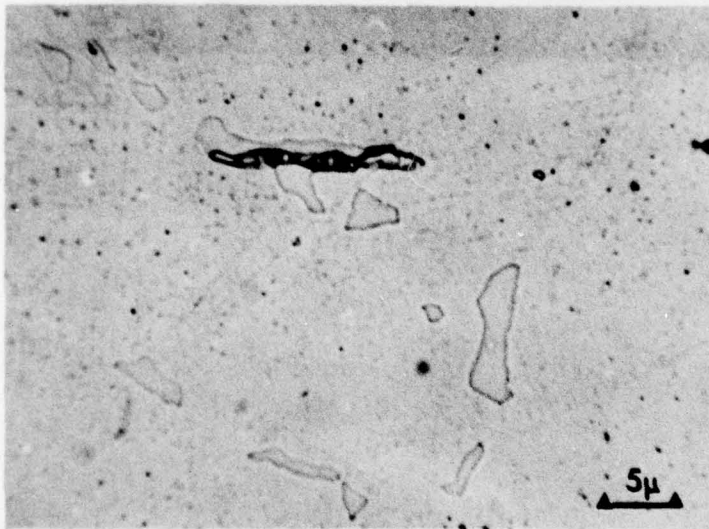


**FIG 8** TYPICAL ELECTRON MICROGRAPH, DIFFRACTION PATTERN AND X-RAY ANALYSIS SPECTRUM OF FERRITE IN 316 ss

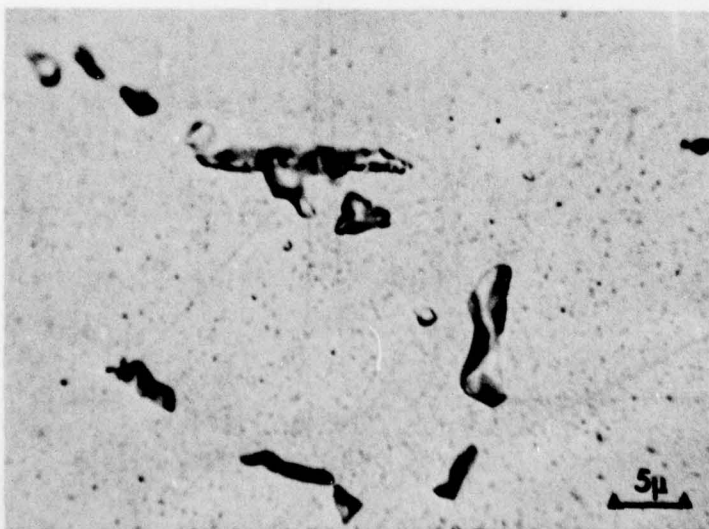


NOMARSKI - as polished



BRIGHT FIELD - as etched

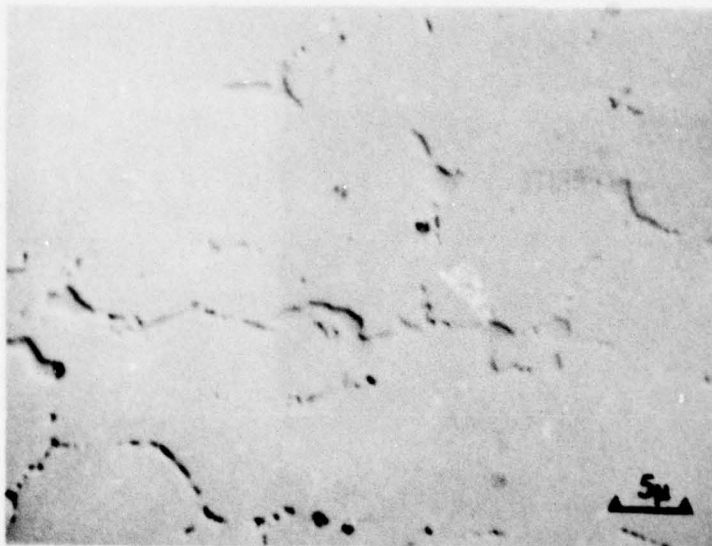
$\frac{1}{2}$  second at  
5 volts in 10%  
oxalic acid



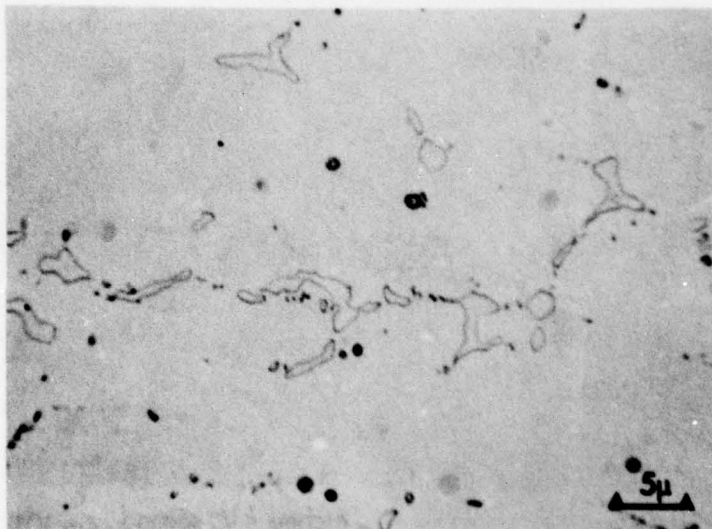
BRIGHT FIELD - as etched

1 second at  
5 volts in 10%  
oxalic acid

**FIG 9** GRAIN BOUNDARY SIGMA PHASE IN 316 ss AGED AT 650°C FOR 22,800h

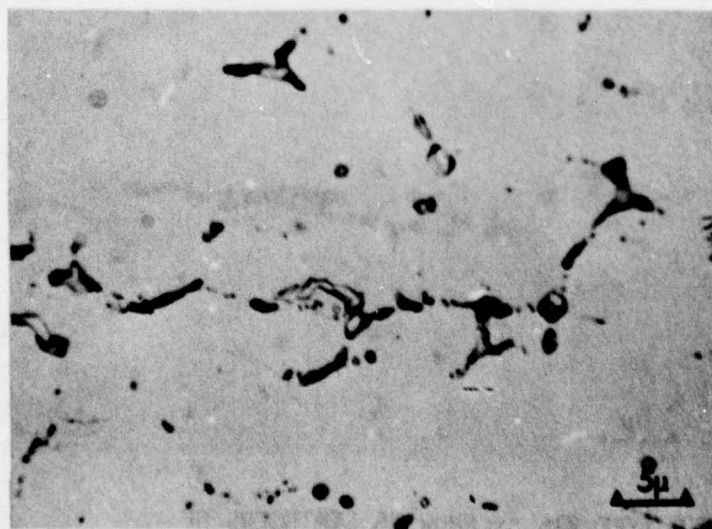


NOMARSKI-as polished



BRIGHT FIELD-as etched

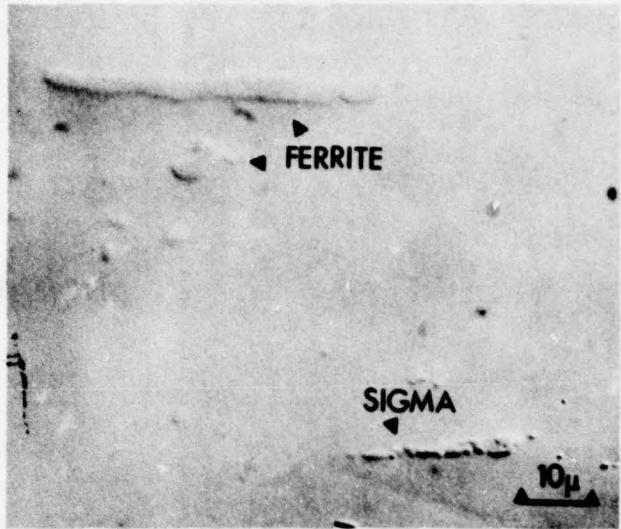
$\frac{1}{2}$  second at  
5volts in 10%  
oxalic acid



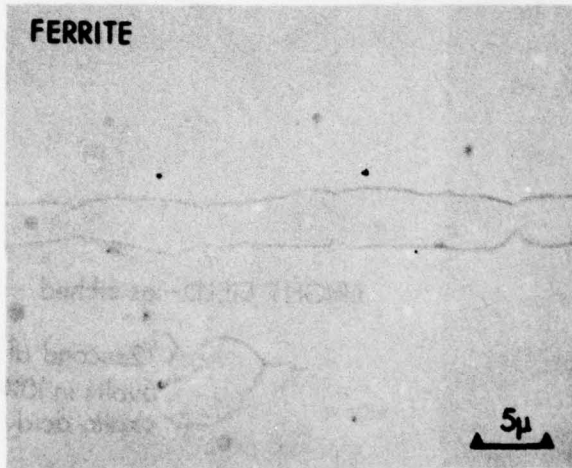
BRIGHT FIELD-as etched

1 second at  
5volts in 10%  
oxalic acid

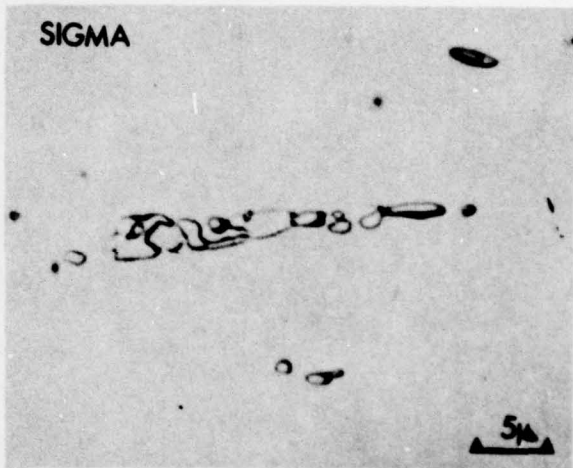
**FIG 10** TYPE 316 ss WELD METAL STRESS RELIEVED AT 850°C FOR 6h  
SHOWING TRANSFORMATION OF THE PRIOR  $\delta$  FERRITE TO SIGMA  
PHASE.



NOMARSKI - as polished



BRIGHT FIELD etched 10seconds in 10%  
etched 20seconds oxalic acid



BRIGHT FIELD etched <math>1/2</math> second in 10%  
etched 1 second oxalic acid

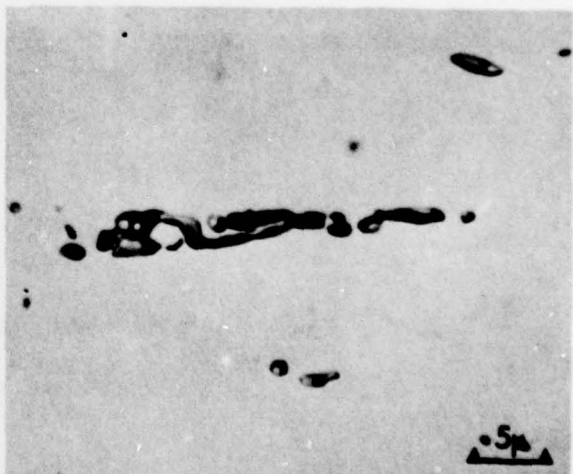
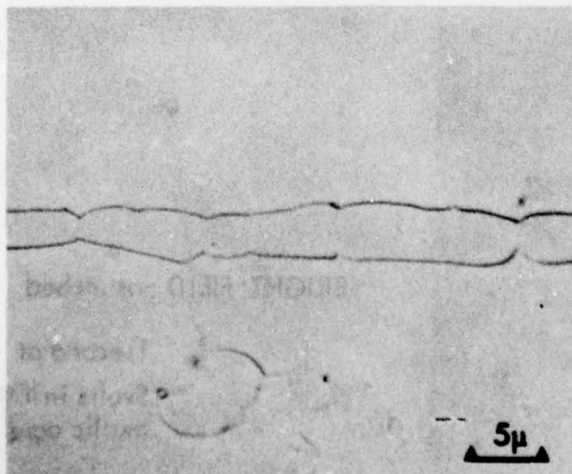
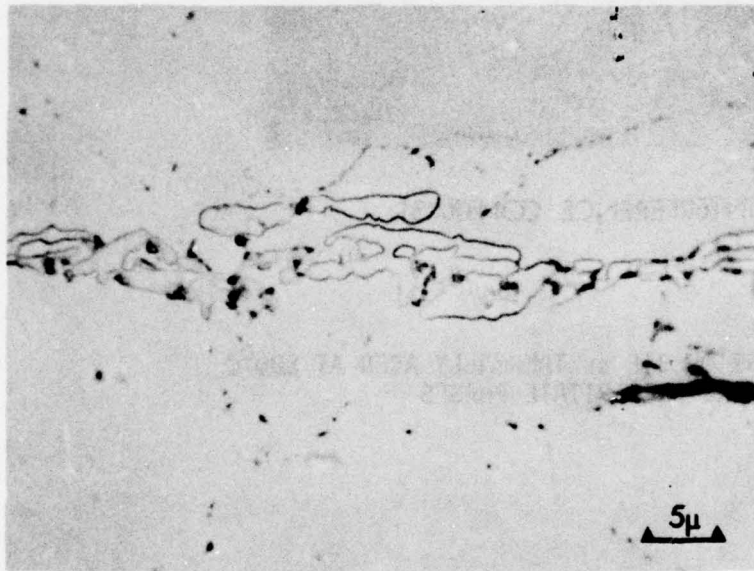


**FIG 11** SOLUTION TREATED TYPE 316 ss SHOWING STRINGERS OF PRIOR  $\delta$  FERRITE AND SIGMA PHASE - CAST PEDIGREE 2

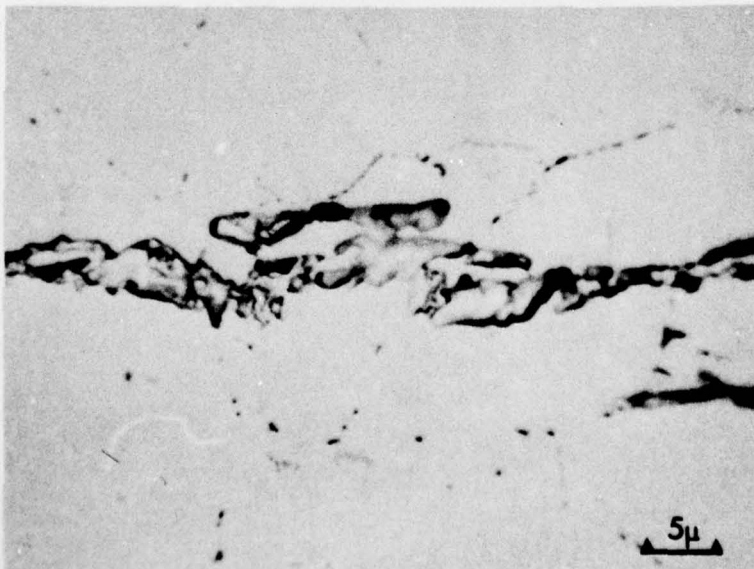


NOMARSKI - as polished



BRIGHT FIELD - as etched

< 1/2 second at  
5 volts in 10%  
oxalic acid

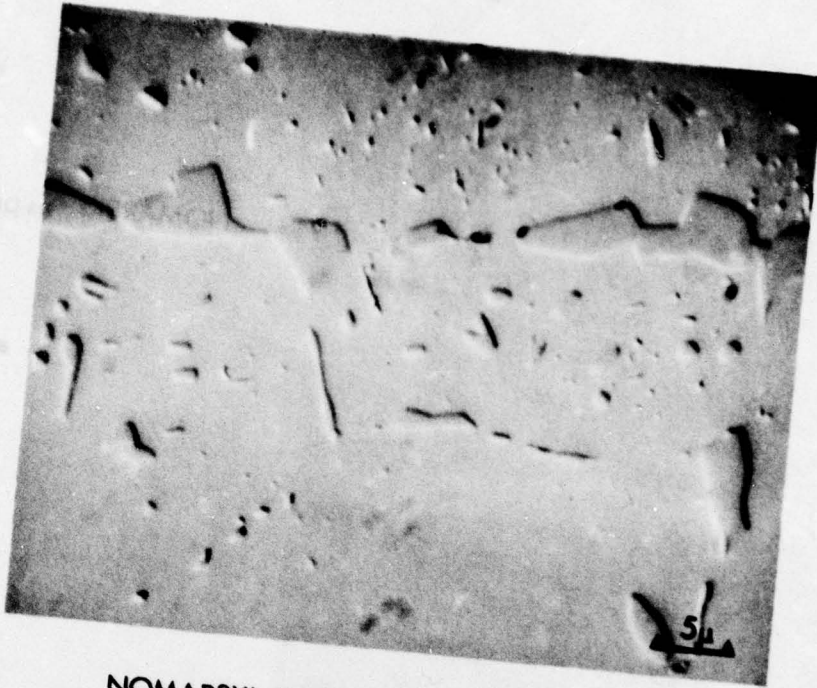


BRIGHT FIELD - as etched

1 second at  
5 volts in 10%  
oxalic acid

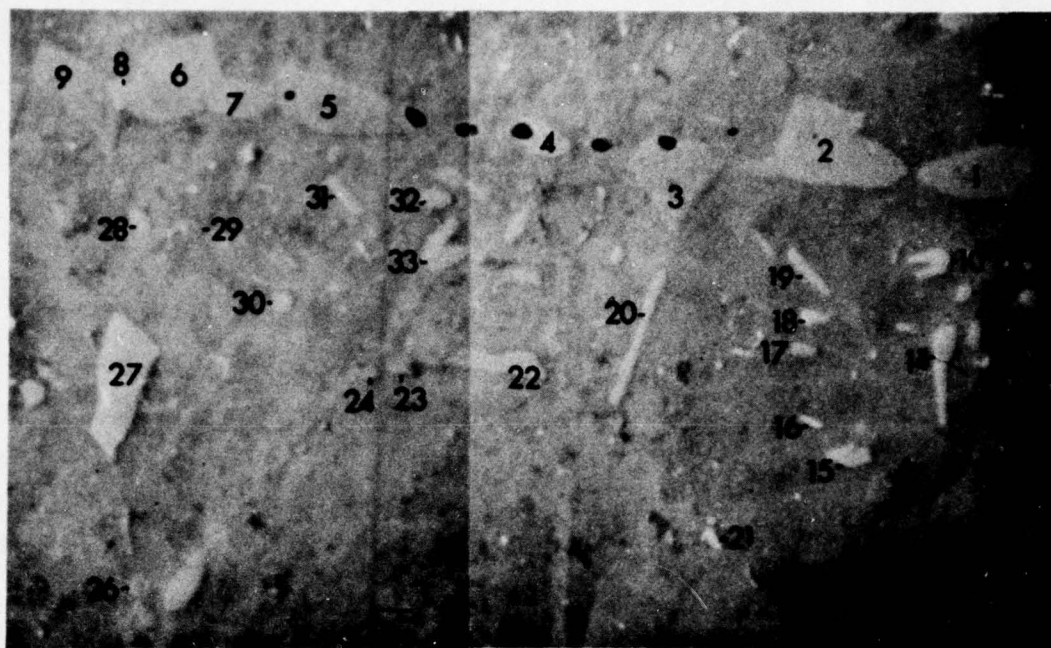
FIG 12

SOLUTION TREATED TYPE 316 ss IN WHICH THE STRINGERS  
HAVE TRANSFORMED TO SIGMA PHASE - CAST PEDIGREE 1



NOMARSKI INTERFERENCE CONTRAST

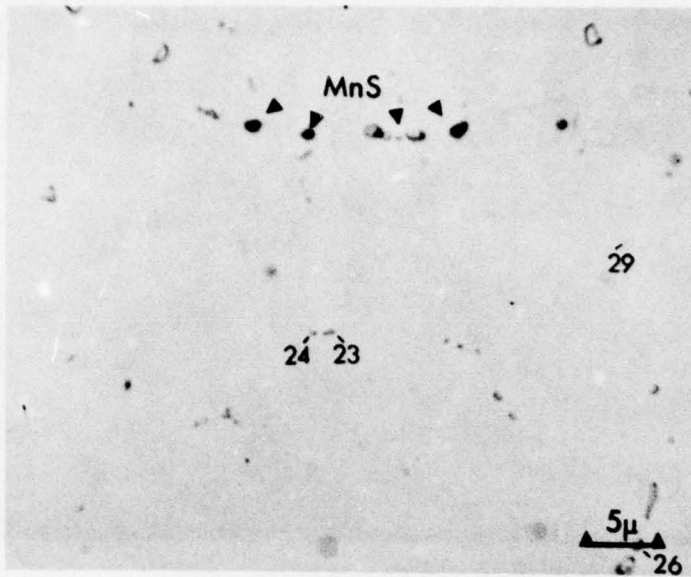
**FIG 13** PEDIGREE 2 CAST OF 316 ss THERMALLY AGED AT 800°C FOR 1000h SHOWING PRECIPITATE PHASES



SECONDARY ELECTRON IMAGE

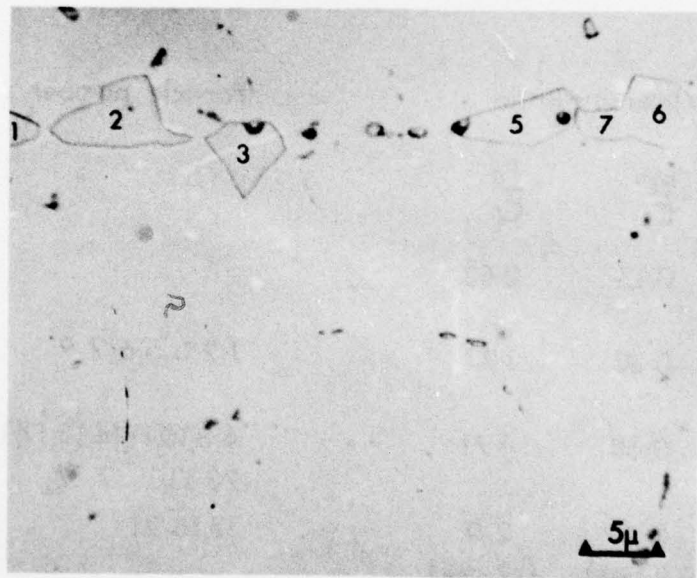
	Intensity Ratio		Particle number
	$\frac{\text{Mo}}{\text{Cr}}$	$\frac{\text{Fe}}{\text{Cr}}$	
Matrix	0.13	2.53	
Sigma	0.30	1.27	1, 2, 3, 5, 6, 7, 9
Chi	0.58	1.71	4, 8, 10, 11, 14, 15, 17, 18, 19, 20, 22, 27, 28, 30, 31, 32, 33
Laves	1.2 (0.9-1.6)	2.0 (1.7-2.4)	13, 16, 21
Carbide	0.14 (0.12-0.18)	0.7 (0.44-0.93)	23, 24, 26, 29

FIG 14 SAME FIELD AS SHOWN IN FIG 13 (MIRROR IMAGE) ILLUSTRATING X-RAY INTENSITY RATIOS FOR SELECTED PARTICLES



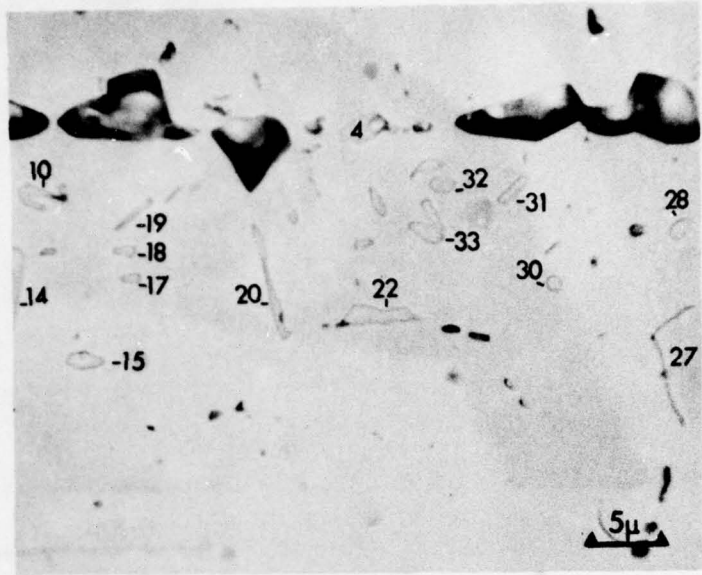
BRIGHT FIELD

**FIG 15** SAME FIELD AS FIG 13 ETCHED IN A 1% SOLUTION OF OXALIC ACID AT 2V FOR  $< \frac{1}{2}$  SEC TO REVEAL CARBIDES. (PARTICLES ANALYSED ARE MARKED (cf FIG 14).)



BRIGHT FIELD

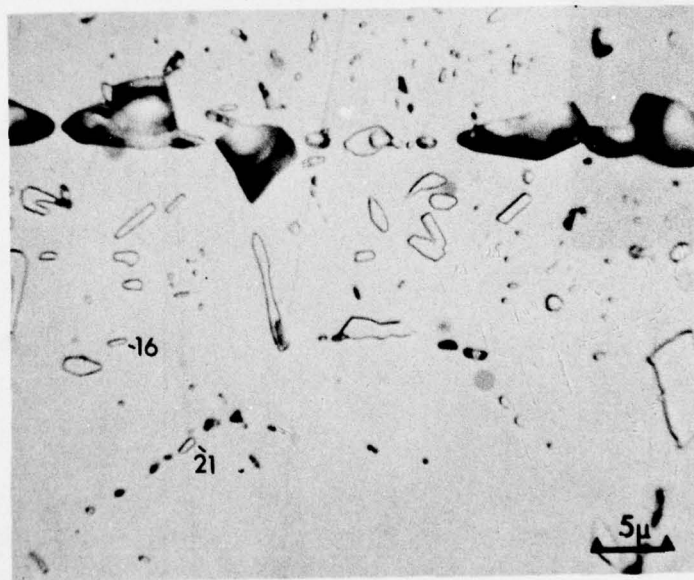
**FIG 16** AS ABOVE PLUS ETCHED IN A 10% SOLUTION OF OXALIC ACID AT 5V FOR  $< \frac{1}{2}$  SEC TO REVEAL SIGMA PHASE. (PARTICLES ANALYSED ARE MARKED (cf FIG 14).)



BRIGHT FIELD

FIG 17

AS FIG 16. ETCHED FOR TOTAL OF 3 SEC IN 10% OXALIC ACID TO REVEAL CHI PHASE. PARTICLES ANALYSED ARE MARKED (cf FIG 14).



BRIGHT FIELD

FIG 18

AS ABOVE ETCHED FOR TOTAL OF 7 SEC AT THIS STAGE LAVES PARTICLES ARE BEING REVEALED BY ETCHANT. (PARTICLES ANALYSED ARE MARKED (cf FIG 14).)



0.5  $\mu$



ZA 210

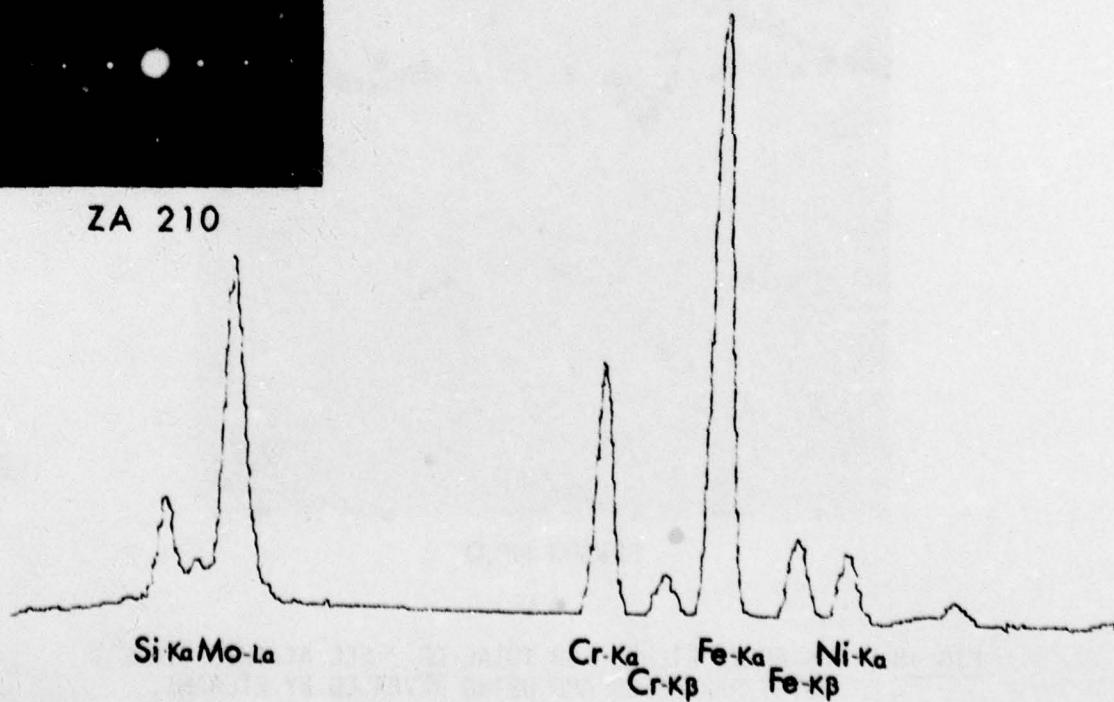
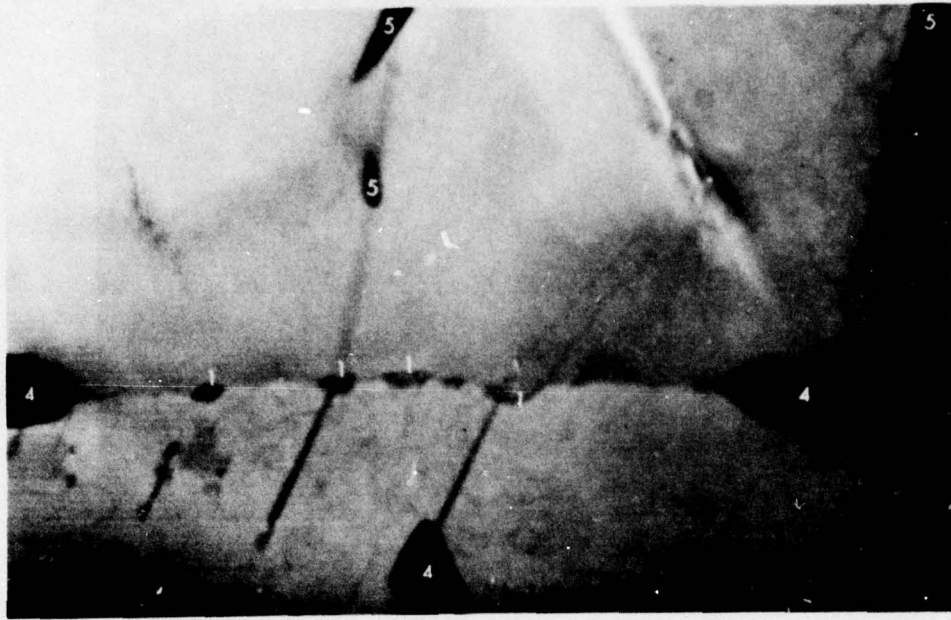
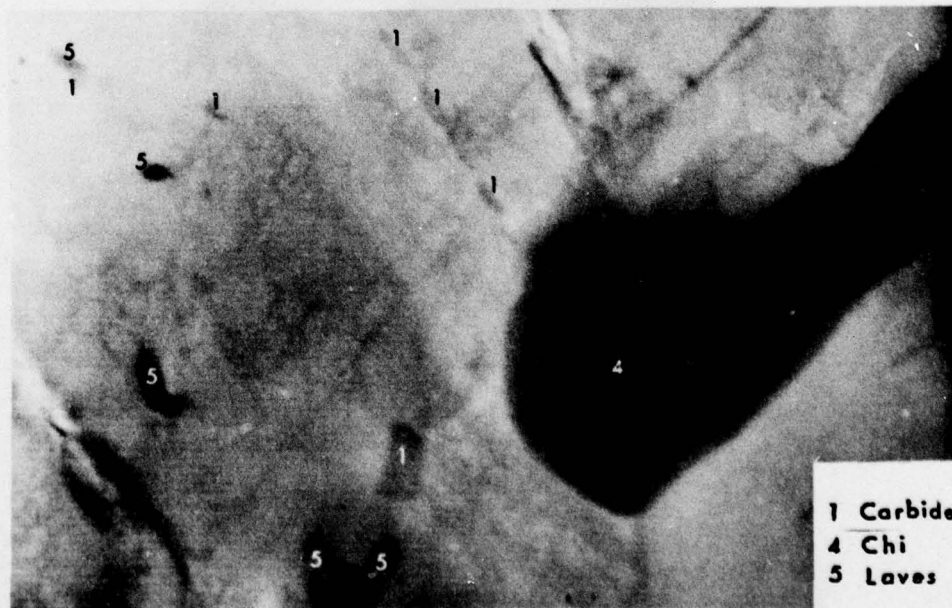


FIG 19

TYPICAL ELECTRON MICROGRAPH, DIFFRACTION PATTERN  
AND X-RAY ANALYSIS SPECTRUM OF LAVES PHASE IN 316 ss



1 μ

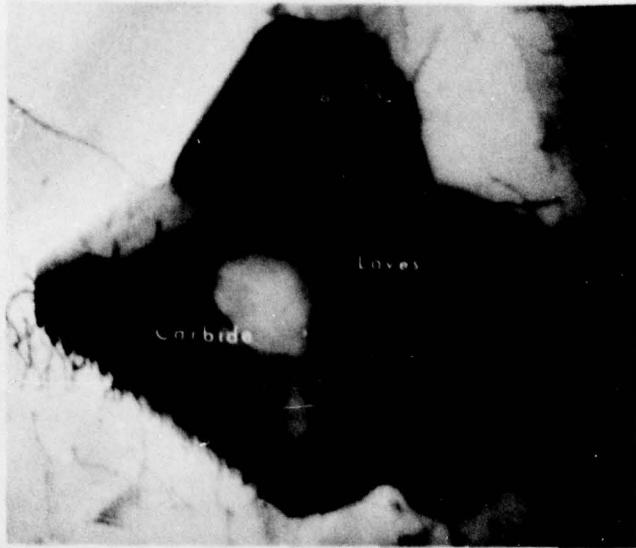


1 Carbide  
4 Chi  
5 Laves

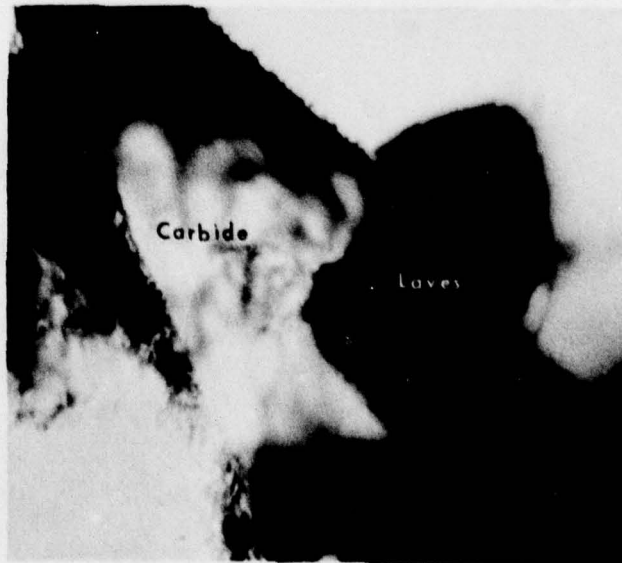
1 μ

**FIG 20**

TYPICAL SCANNING TRANSMISSION ELECTRON MICROGRAPHS OF PEDIGREE 2 CAST OF 316 ss AGED 1000h AT 800°C



0.5μ



0.5μ

FIG 21

EXAMPLES OF 2-PHASE CARBIDE AND LAVES PRECIPITATES  
CO-EXISTING IN PEDIGREE 1 CAST OF 316 ss AGED 1000h  
AT 800°C